Experimental Investigation of Fundamental Properties of Snake Robot Locomotion

Pål Liljebäck[1,2], Kristin Y. Pettersen[1], Øyvind Stavdahl[1], Jan Tommy Gravdahl[1]
[1]Norwegian University of Science and Technology, Dept. of Engineering Cybernetics, NO-7491 Trondheim, Norway
[2]SINTEF ICT, Dept. of Applied Cybernetics, N-7465 Trondheim, Norway
E-mail addresses: Pal.Liljeback@sintef.no, {Kristin.Y.Pettersen, Oyvind.Stavdahl, Tommy.Gravdahl}@itk.ntnu.no

***Abstract*—This paper derives and experimentally investigates fundamental properties of the velocity of a snake robot conducting lateral undulation. In particular, the derived properties state that the average forward velocity of the snake robot 1) is proportional to the squared amplitude of the sinusoidal motion of each joint of the robot, 2) is proportional to the angular frequency of the sinusoidal motion of each joint, 3) is proportional to a particular function of the constant phase shift between the joints, and 4) is maximized by the phase shift between the joints that also maximizes the particular phase shift function. The paper presents an experimental investigation of the validity of these derived properties by measuring the forward velocity of a physical snake robot during lateral undulation. The experimental results support the theoretical findings.**

***Index Terms*—Snake robot, Averaging, Stability analysis, Velocity dynamics.**

I. Introduction

Inspired by biological snakes, snake robots carry the potential of meeting the growing need for robotic mobility in challenging environments. Snake robots consist of serially connected modules capable of bending in one or more planes. The many degrees of freedom of snake robots make them difficult to control, but provide traversability in irregular environments that surpasses the mobility of the more conventional wheeled, tracked and legged forms of robotic mobility. Research on snake robots has been conducted for several decades. However, our understanding of snake locomotion so far is for the most part based on empirical studies of biological snakes and simulation-based synthesis of relationships between parameters of the snake robot.

There are several reported works aimed at analysing and understanding snake locomotion. Gray [1] conducted empirical and analytical studies of snake locomotion already in the 1940s. Hirose [2] studied biological snakes and developed mathematical relationships characterizing their motion, such as the *serpenoid curve*. Saito *et al.* [3] optimized the parameters of the serpenoid curve based on simulations of a planar snake robot. Hicks [4] investigated general requirements for the propulsion of a three-linked snake robot. Nilsson [5] employed energy arguments to analyse planar snake locomotion with isotropic friction. Transeth *et al.* [6] proved that the velocity of a planar snake robot is bounded. Li *et al.* [7] studied the controllability of the joint motion of a snake robot. The authors have previously studied the stability properties of snake locomotion based on *Poincaré maps* [8] and investigated the controllability properties of a planar snake robot influenced by anisotropic friction [9].

Research on robotic fish and eel-like mechanisms is relevant to research on snake robots since these mechanisms are very similar. The works in [10]–[12] investigate the controllability of various fish-like mechanisms, synthesize gaits for translational and rotational motion based on Lie bracket calculations, and propose controllers for tracking straight and curved trajectories.

The contribution of this paper is the derivation and experimental investigation of a set of fundamental properties of the velocity dynamics of a planar snake robot that are useful from a motion planning perspective. The properties are derived based on a simplified model of a snake robot proposed by the authors in [13]. The derived properties state that the average forward velocity of a planar snake robot 1) is proportional to the squared amplitude of the sinusoidal motion of each joint of the robot, 2) is proportional to the angular frequency of the sinusoidal motion of each joint, 3) is proportional to a particular function of the constant phase shift between the joints, and 4) is maximized by the phase shift between the joints that also maximizes the particular phase shift function. A derivation of these properties is also presented in [14], but whereas the properties are supported by simulation results in [14], this paper investigates the validity of the properties through experiments with a physical snake robot. The experimental results support the derived properties of the velocity dynamics.

The paper is organized as follows. Section II presents a simplified model of a snake robot that the theoretical findings are based upon. Section III presents a controller for the snake robot. Section IV derives fundamental properties of the velocity dynamics of the snake robot. Section V describes the experimental setup employed in order to investigate the validity of the theoretical results. Section VI presents the experimental results. Finally, Section VII presents concluding remarks.

II. A model of the snake robot

This section summarizes a model of a planar snake robot which is described in detail in [13]. The model forms the basis of the investigation of the fundamental locomotion properties in Section IV.

A. Overview of the model

We consider a planar snake robot with links interconnected by active revolute joints. The surface beneath the robot is flat and horizontal, and each link is subjected to a viscous ground friction force. The body shape changes of the robot induce

978-1-4244-7815-6/10/$26.00

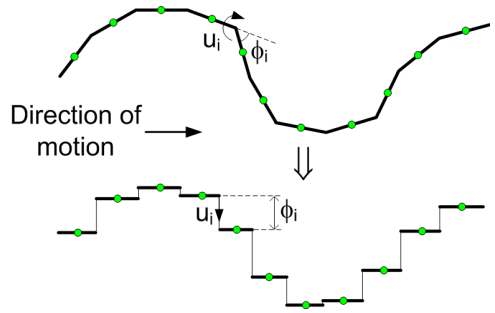

Fig. 1. The revolute joints of the snake robot are modelled as prismatic joints that displace the CM of each link transversal to the direction of motion.

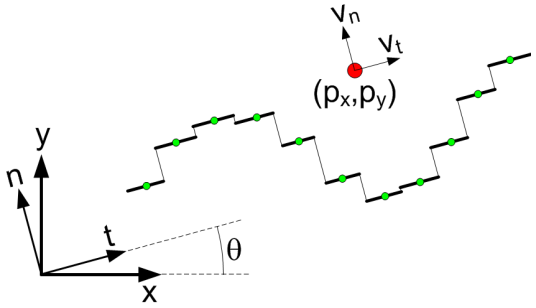

Fig. 2. Illustration of the two coordinate frames employed in the model. The global x-y frame is fixed. The t-n frame is always aligned with the snake robot.

friction forces on the links that produce the translational and rotational motion of the robot. A simplified model that captures only the most essential part of the snake robot dynamics is proposed in [13]. The idea behind this model is illustrated in Fig. 1 and motivated by an analysis presented in [13], which shows that:

- The forward motion of a planar snake robot is produced by the link velocity components that are *normal* to the forward direction.
- The change in body shape during forward locomotion primarily consists of relative displacements of the CM of the links *normal* to the forward direction of motion.

Based on these two properties, the simplified model describes the body shape changes of a snake robot as *linear displacements* of the links with respect to each other instead of rotational displacements. The linear displacements occur *normal* to the forward direction of motion and produce friction forces that propel the robot forward. This essentially means that the revolute joints of the snake robot are modelled as prismatic (translational) joints and that the rotational motion of the links during body shape changes is disregarded. However, the model still captures the *effect* of the rotational link motion during body shape changes, which is a linear displacement of the CM of the links normal to the forward direction of motion.

The model of the snake robot is summarized in the following subsections in terms of the symbols illustrated in Fig. 2 and Fig. 3.

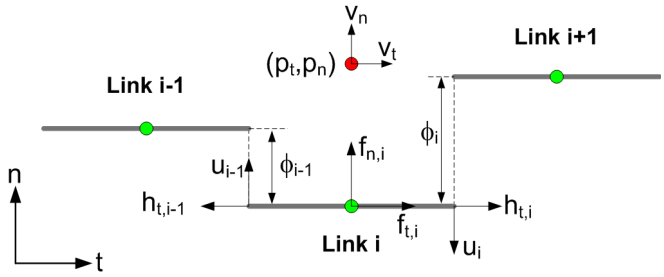

Fig. 3. Symbols characterizing the kinematics and dynamics of the snake robot.

B. Kinematics of the snake robot

The snake robot has N links of length l and mass m interconnected by $N-1$ prismatic joints. The prismatic joints control the normal direction distance between the links. As seen in Fig. 3, the normal direction distance from link i to link $i+1$ is denoted by ϕ_i and represents the coordinate of joint i. The positive direction of ϕ_i is along the n axis.

The snake robot moves in the horizontal plane and has $N+2$ degrees of freedom. The motion is defined with respect to the two coordinate frames illustrated in Fig. 2. The x-y frame is the fixed global frame. The t-n frame is always aligned with the snake robot, i.e. the t and n axis always point in the *tangential* and *normal* direction of the robot, respectively. The origin of both frames are fixed and coincide.

As seen in Fig. 2 and Fig. 3, the global frame position of the CM (center of mass) of the snake robot is denoted by $(p_x, p_y) \in \mathbb{R}^2$, while the t-n frame position is denoted by $(p_t, p_n) \in \mathbb{R}^2$. The global frame orientation is denoted by $\theta \in \mathbb{R}$ and is expressed with respect to the global x axis with counterclockwise positive direction. The angle between the global x axis and the t axis is also θ since the t-n frame is always aligned with the snake robot. The relationship between the t-n frame and the global frame position is given by

$$p_t = p_x \cos\theta + p_y \sin\theta \tag{1a}$$
$$p_n = -p_x \sin\theta + p_y \cos\theta \tag{1b}$$

C. Equations of motion

The state vector of the model is chosen as

$$\boldsymbol{x} = (\boldsymbol{\phi}, \theta, p_t, p_n, \boldsymbol{v}_\phi, v_\theta, v_t, v_n) \in \mathbb{R}^{2N+4} \tag{2}$$

where $\boldsymbol{\phi} = (\phi_1, \cdots, \phi_{N-1}) \in \mathbb{R}^{N-1}$ are the joint coordinates, $\theta \in \mathbb{R}$ is the absolute orientation, $(p_t, p_n) \in \mathbb{R}^2$ is the t-n frame position of the CM, $\boldsymbol{v}_\phi = \dot{\boldsymbol{\phi}} \in \mathbb{R}^{N-1}$ are the joint velocities, $v_\theta = \dot{\theta} \in \mathbb{R}$ is the angular velocity, and $(v_t, v_n) \in \mathbb{R}^2$ is the tangential and normal direction velocity of the snake robot.

As illustrated in Fig. 3, each link is influenced by a ground friction force (acting on the CM of the link) and constraint forces that hold the joints together. A model of these forces is presented in [13], where it is also shown that the complete

model of the snake robot can be written as

$$\dot{\boldsymbol{\phi}} = \boldsymbol{v}_\phi \tag{3a}$$
$$\dot{\theta} = v_\theta \tag{3b}$$
$$\dot{p}_t = v_t + p_n v_\theta \tag{3c}$$
$$\dot{p}_n = v_n - p_t v_\theta \tag{3d}$$
$$\dot{\boldsymbol{v}}_\phi = -\frac{c_1}{m}\boldsymbol{v}_\phi + \frac{c_2}{m} v_t \boldsymbol{A}\boldsymbol{D}^T\boldsymbol{\phi} + \frac{1}{m}\boldsymbol{D}\boldsymbol{D}^T\boldsymbol{u} \tag{3e}$$
$$\dot{v}_\theta = -c_3 v_\theta + \frac{c_4}{N-1} v_t \overline{\boldsymbol{e}}^T\boldsymbol{\phi} \tag{3f}$$
$$\dot{v}_t = -\frac{c_1}{m}v_t + \frac{2c_2}{Nm} v_n \overline{\boldsymbol{e}}^T\boldsymbol{\phi} - \frac{c_2}{Nm}\boldsymbol{\phi}^T\boldsymbol{A}\overline{\boldsymbol{D}}\boldsymbol{v}_\phi \tag{3g}$$
$$\dot{v}_n = -\frac{c_1}{m}v_n + \frac{2c_2}{Nm} v_t \overline{\boldsymbol{e}}^T\boldsymbol{\phi} \tag{3h}$$

where $\boldsymbol{u} \in \mathbb{R}^{N-1}$ are the actuator forces at the joints and $\overline{\boldsymbol{e}} = \begin{bmatrix}1 & . & . & 1\end{bmatrix}^T \in \mathbb{R}^{N-1}$, $\overline{\boldsymbol{D}} = \boldsymbol{D}^T\left(\boldsymbol{D}\boldsymbol{D}^T\right)^{-1} \in \mathbb{R}^{N\times(N-1)}$,

$$\boldsymbol{A} = \begin{bmatrix}1 & 1 & & \\ & . & . & \\ & & . & . \\ & & 1 & 1\end{bmatrix}, \boldsymbol{D} = \begin{bmatrix}1 & -1 & & \\ & . & . & \\ & & . & . \\ & & 1 & -1\end{bmatrix},$$

where $\boldsymbol{A} \in \mathbb{R}^{(N-1)\times N}$ and $\boldsymbol{D} \in \mathbb{R}^{(N-1)\times N}$. The parameters c_1, c_2, c_3, and c_4 are scalar friction coefficients that characterize the external forces acting on the snake robot. More specifically, the coefficient c_1 determines the magnitude of the friction forces resisting the link motion, c_2 determines the magnitude of the induced friction forces that propel the snake robot forward, c_3 determines the friction torque opposing the rotation of the snake robot, while c_4 determines the induced torque that rotates the snake robot. This torque is induced when the forward direction velocity and the average of the joint coordinates are nonzero. The role of each coefficient is explained in more detail in [13].

III. Controller design

The actuator forces are set according to the linearizing control law

$$\boldsymbol{u} = m\left(\boldsymbol{D}\boldsymbol{D}^T\right)^{-1}\left(\overline{\boldsymbol{u}} + \frac{c_1}{m}\dot{\boldsymbol{\phi}} - \frac{c_2}{m} v_t \boldsymbol{A}\boldsymbol{D}^T\boldsymbol{\phi}\right) \tag{4}$$

where $\overline{\boldsymbol{u}} \in \mathbb{R}^{N-1}$ is a new set of control inputs. This control law transforms the joint dynamics (3e) into $\dot{\boldsymbol{v}}_\phi = \overline{\boldsymbol{u}}$.

We will control the snake robot according to a motion pattern called *lateral undulation* [2], which consists of horizontal waves that are propagated backwards along the snake body from head to tail. Lateral undulation is achieved by controlling joint $i \in \{1, \cdots, N-1\}$ of the snake robot according to the sinusoidal reference

$$\phi_{i,\mathrm{ref}} = \alpha \sin\left(\omega t + (i-1)\,\delta\right) + \phi_o \tag{5}$$

where α and ω are the amplitude and frequency, respectively, of the sinusoidal joint motion and δ determines the phase shift between the joints. The parameter ϕ_o is a joint offset coordinate used to control the direction of the locomotion. We assume that ϕ_o is a constant offset, so that

$$\dot{\phi}_{i,\mathrm{ref}} = \alpha\omega \cos\left(\omega t + (i-1)\,\delta\right) \tag{6}$$
$$\ddot{\phi}_{i,\mathrm{ref}} = -\alpha\omega^2 \sin\left(\omega t + (i-1)\,\delta\right) \tag{7}$$

We choose the control input $\overline{\boldsymbol{u}}$ of the snake robot as

$$\overline{\boldsymbol{u}} = \ddot{\boldsymbol{\phi}}_{\mathrm{ref}} + k_d\left(\dot{\boldsymbol{\phi}}_{\mathrm{ref}} - \dot{\boldsymbol{\phi}}\right) + k_p\left(\boldsymbol{\phi}_{\mathrm{ref}} - \boldsymbol{\phi}\right) \tag{8}$$

where k_p and k_d are positive scalar controller gains and $\boldsymbol{\phi}_{\mathrm{ref}} \in \mathbb{R}^{N-1}$ are the joint reference coordinates. The error dynamics of the joints is therefore given by

$$\left(\ddot{\boldsymbol{\phi}}_{\mathrm{ref}} - \ddot{\boldsymbol{\phi}}\right) + k_d\left(\dot{\boldsymbol{\phi}}_{\mathrm{ref}} - \dot{\boldsymbol{\phi}}\right) + k_p\left(\boldsymbol{\phi}_{\mathrm{ref}} - \boldsymbol{\phi}\right) = 0 \tag{9}$$

which is clearly *exponentially stable* [15].

IV. Analysis of the velocity dynamics based on averaging theory

In this section, *averaging theory* [16] is employed in order to study the velocity dynamics of the snake robot during lateral undulation. We employ averaging theory since we are primarily interested in the overall, i.e. average, speed and direction of the locomotion. The periodic fluctuations about the average trajectory of the snake is not of particular interest.

A. Model of the velocity dynamics of the snake robot

The velocity dynamics of the snake robot is defined by (3f), (3g), and (3h), which give the dynamics of the forward direction velocity v_t, the normal direction velocity v_n, and the angular velocity v_θ of the snake robot. It was shown in Section III that we can achieve exponentially stable tracking of the joint reference coordinates (5) with the control law (8). We will therefore assume that $\boldsymbol{\phi}$ and $\boldsymbol{v}_\phi = \dot{\boldsymbol{\phi}}$ are given by (5) and (6), respectively. Furthermore, we assume that the amplitude α and frequency ω of the joint motion are always set according to the rule

$$\omega = \frac{k_{\alpha\omega}}{\alpha^2} \tag{10}$$

where $k_{\alpha\omega} > 0$ is a constant controller parameter. This rule allows us to write the model of the velocity dynamics in a particular standard averaging form in the next subsection. Note that α and ω are still independent parameters since any choice of α and ω can be obtained by choosing $k_{\alpha\omega} = \alpha^2\omega$. Using (5), (6), and (10), and introducing the velocity state vector $\boldsymbol{v} = (v_t, v_n, v_\theta) \in \mathbb{R}^3$, the velocity dynamics can be written as

$$\dot{\boldsymbol{v}} = \begin{bmatrix}\dot{v}_t \\ \dot{v}_n \\ \dot{v}_\theta\end{bmatrix} = \boldsymbol{f}\left(t, \boldsymbol{v}\right) \tag{11}$$

where

$$\boldsymbol{f}\left(t,\boldsymbol{v}\right) = \begin{bmatrix}-\frac{c_1}{m}v_t + \frac{2c_2}{Nm}v_n f_1\left(\omega t\right) - \frac{c_2}{Nm} f_2\left(\omega t\right) \\ -\frac{c_1}{m}v_n + \frac{2c_2}{Nm}v_t f_1\left(\omega t\right) \\ -c_3 v_\theta + \frac{c_4}{N-1} v_t f_1\left(\omega t\right)\end{bmatrix} \tag{12}$$

$$f_1\left(\omega t\right) = \left(N-1\right)\phi_o + \sum_{i=1}^{N-1}\alpha\sin\left(\omega t + (i-1)\,\delta\right) \tag{13}$$

$$\begin{aligned} f_2\left(\omega t\right) = \sum_{i=1}^{N-1}\sum_{j=1}^{N-1}\big[&\tfrac{k_{\alpha\omega}}{\alpha}\phi_o a_{ij}\cos\left(\omega t + (j-1)\,\delta\right) \\ &+ k_{\alpha\omega} a_{ij}\sin\left(\omega t + (i-1)\,\delta\right)\cos\left(\omega t + (j-1)\,\delta\right)\big] \end{aligned} \tag{14}$$

and where a_{ij} denotes element ij of the matrix $\boldsymbol{A}\overline{\boldsymbol{D}}$.

B. Averaged model of the velocity dynamics

The method of *averaging* [16] can be applied to systems of the form

$$\dot{\boldsymbol{x}} = \varepsilon \boldsymbol{f}(t, \boldsymbol{x}) \tag{15}$$

where $\varepsilon > 0$ is a small parameter and $\boldsymbol{f}(t, \boldsymbol{x})$ is T-periodic, i.e. $\boldsymbol{f}(t+T, \boldsymbol{x}) = \boldsymbol{f}(t, \boldsymbol{x})$. A system that, in 'average', behaves similarly to the system in (15) is given by

$$\dot{\boldsymbol{x}} = \varepsilon \frac{1}{T} \int_0^T \boldsymbol{f}(\tau, \boldsymbol{x})\, d\tau \tag{16}$$

The smallness requirement on ε ensures that $\boldsymbol{x}$ varies slowly with t relative to the periodic excitation of the system. The system response will thereby be determined predominantly by the average of the excitation.

To transform the model (11) into the standard form of averaging (15), we change the time scale from t to $\tau = \omega t$ and define $\varepsilon = 1/\omega$. Since $\frac{d}{dt} = \frac{1}{\varepsilon}\frac{d}{d\tau}$, the model (11) can now be written as

$$\frac{d\boldsymbol{v}}{d\tau} = \varepsilon \boldsymbol{f}(\tau, \boldsymbol{v}) \tag{17}$$

where

$$\boldsymbol{f}(\tau, \boldsymbol{v}) = \begin{bmatrix} -\frac{c_1}{m} v_t + \frac{2c_2}{Nm} v_n f_1(\tau) - \frac{c_2}{Nm} f_2(\tau) \\ -\frac{c_1}{m} v_n + \frac{2c_2}{Nm} v_t f_1(\tau) \\ -c_3 v_\theta + \frac{c_4}{N-1} v_t f_1(\tau) \end{bmatrix} \tag{18}$$

The averaged model of (17) is now given by calculating the integral in (16) and changing time scale back to t using that $\frac{d}{d\tau} = \varepsilon \frac{d}{dt}$. The resulting averaged model is shown in [17] to be given by

$$\dot{\boldsymbol{v}} = \mathcal{A}\boldsymbol{v} + \boldsymbol{b} \tag{19}$$

where

$$\mathcal{A} = \mathcal{A}(\phi_o) = \begin{bmatrix} -\frac{c_1}{m} & \frac{2(N-1)}{Nm} c_2 \phi_o & 0 \\ \frac{2(N-1)}{Nm} c_2 \phi_o & -\frac{c_1}{m} & 0 \\ c_4 \phi_o & 0 & -c_3 \end{bmatrix} \tag{20}$$

$$\boldsymbol{b} = \boldsymbol{b}(\alpha, \omega, \delta) = \begin{bmatrix} \frac{c_2}{2Nm} k_{\alpha\omega} k_\delta \\ 0 \\ 0 \end{bmatrix} \tag{21}$$

and where the constant $k_\delta \in \mathbb{R}$ is defined as

$$k_\delta = \sum_{i=1}^{N-1} \sum_{j=1}^{N-1} a_{ij} \sin((j-i)\delta) \tag{22}$$

We see that the averaged model of the velocity dynamics is a linear system characterized by the parameters of the joint reference coordinates, i.e. by α, ω, δ, and ϕ_o.

C. Analysis of the velocity dynamics

The averaged model (19) has a single equilibrium point at $\boldsymbol{v} = -\mathcal{A}^{-1}\boldsymbol{b}$. By inspecting the eigenvalues of $\mathcal{A}$, it is shown in [17] that this equilibrium point is *globally exponentially stable* as long as the joint coordinate offset ϕ_o is below a certain threshold. This means that the average velocity of the snake robot will converge exponentially to the steady state velocity

$$\overline{\boldsymbol{v}} = -\mathcal{A}^{-1}\boldsymbol{b} = \begin{bmatrix} \overline{v}_t & \overline{v}_n & \overline{v}_\theta \end{bmatrix}^T \tag{23}$$

which is given analytically by

$$\overline{v}_t = k_{\alpha\omega} k_\delta \frac{N c_1 c_2}{2\left(N^2 c_1^2 - (4N^2 - 8N + 4) c_2^2 \phi_o^2\right)} \tag{24a}$$

$$\overline{v}_n = k_{\alpha\omega} k_\delta \frac{\phi_o (N-1) c_2^2}{N^2 c_1^2 - (4N^2 - 8N + 4) c_2^2 \phi_o^2} \tag{24b}$$

$$\overline{v}_\theta = k_{\alpha\omega} k_\delta \frac{\phi_o N c_1 c_2 c_4}{2c_3 (N^2 c_1^2 - (4N^2 - 8N + 4) c_2^2 \phi_o^2)} \tag{24c}$$

The work in [17] provides more details regarding the correspondence between the average and the exact velocity of the snake robot. The main result in [17] is basically that, for sufficiently large ω, the average velocity of the snake robot given by (19) will approximate the exact velocity given by (11) for all time, and the error of this approximation is bounded.

Eq. (23) represents an interesting result since it gives an analytical expression for the steady state velocity of a snake robot with an arbitrary number of links N as a function of the controller parameters α, ω, δ, and ϕ_o. We can for example immediately see that the steady state velocity of the snake robot when it conducts lateral undulation with zero joint offset ($\phi_o = 0$) is given by $\overline{v}_t = \frac{c_2}{2Nc_1} k_{\alpha\omega} k_\delta$, $\overline{v}_n = 0$, and $\overline{v}_\theta = 0$. In the following, we will use this result to deduce some fundamental relationships between the forward velocity and the controller parameters of the snake robot.

The forward velocity is seen from (24a) to be proportional to the controller parameter $k_{\alpha\omega} = \alpha^2\omega$, i.e. the forward velocity is proportional to the square of the amplitude of the joint motion, α^2, and also proportional to the angular frequency, ω, of the joint motion. This information is useful from a motion planning perspective since it tells us that an increase/decrease of the forward velocity by a certain factor can be achieved by increasing/decreasing ω by the same factor or by increasing/decreasing α by the square root of this factor.

It is also seen from (24a) that the forward velocity of the snake robot is proportional to the function k_δ defined in (22). Since k_δ is a function of the phase shift δ between the joints, this means that the phase shift δ that will maximize the forward velocity can be determined analytically as the δ that maximizes k_δ. This is particularly interesting since we are now able to analytically determine the optimal phase shift δ that maximizes the forward velocity of a planar snake robot with an arbitrary number of links N. Fig. 4 presents a plot of the maximum value of k_δ as a function of the number of links N. For each N, the maximum value of k_δ was found using the mathematical computer software *Matlab*. The optimal phase shift is e.g. $\delta = 90^\circ$ for $N = 3$ links, $\delta = 50.4^\circ$ for $N = 5$ links, $\delta = 24.1^\circ$ for $N = 10$ links, and $\delta = 11.5^\circ$ for $N = 20$ links.

The above results can be summarized as follows:

Proposition 1: Consider a planar snake robot with N links modelled by (3) and controlled in exact accordance with (5) and (6). The average forward velocity of the snake robot given by (19) will converge exponentially to a value which is proportional to:
- the squared amplitude of the sinusoidal joint motion, α^2.
- the angular frequency of the sinusoidal joint motion, ω.
- the function of the constant phase shift, δ, between the joints given by

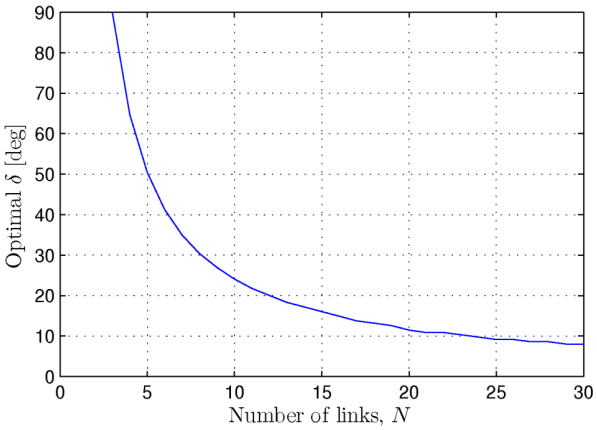

Fig. 4. The optimal phase shift δ that maximizes the forward velocity of a planar snake robot as a function of the number of links N.

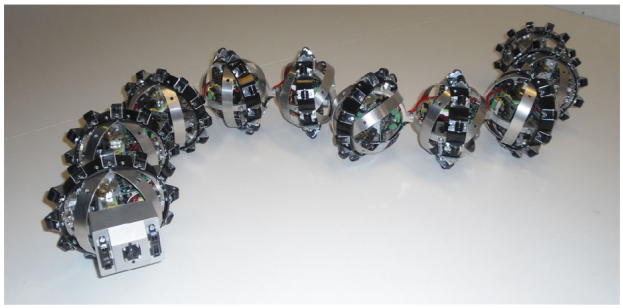

Fig. 5. The snake robot used in the experiments.

$$k_\delta = \sum_{i=1}^{N-1}\sum_{j=1}^{N-1} a_{ij} \sin\left((j-i)\,\delta\right) \tag{25}$$

where a_{ij} denotes element ij of the matrix $A\overline{D}$. Moreover, for a given α and ω, the phase shift, δ, that maximizes the average forward velocity is given by the δ that maximizes k_δ.

V. Experimental Setup

This section describes the experimental setup employed in order to investigate the validity of the results stated in Proposition 1.

A. The snake robot

The snake robot used in the experiments is shown in Fig. 5. A detailed description of the internal components of the robot is given in [18].

The snake robot consists of 10 identical joint modules characterized by the parameters listed in Table I. The articulation mechanism of a joint module is shown in Fig. 6 and consists of two links that can move in pitch and yaw, respectively. The links are supported by bearings in a steel ring and have orthogonal and intersecting axes of rotation. The diameter of the steel ring is 130 mm. Each link is driven by a Hitec servo motor (HS-5955TG) and the angle of the links are measured with magnetic rotary encoders (AS5043 from austriamicrosystems).

TABLE I
Parameters of a joint module.

Parameter	**Value**
Total weight of a joint module	960 g
Outer diameter	130 mm
Degrees of freedom	2
Max joint travel	$\pm 45^\circ$
Max continuous joint torque	4.5 Nm
Max joint speed (no load)	$70^\circ/_{\text{sec}}$

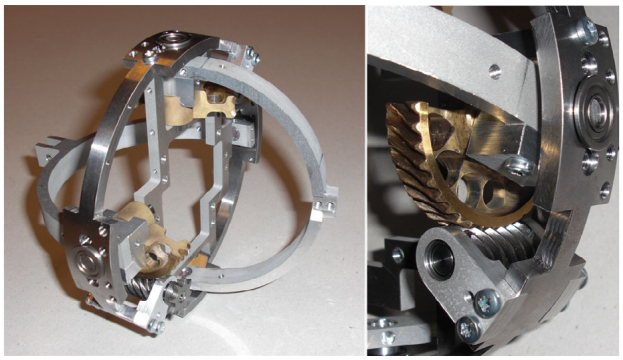

Fig. 6. The articulation mechanism of the snake robot.

As shown in Fig. 7, each joint module of the robot is enclosed by a plastic ring mounted with 12 plastic wheels. These wheels ensure that the ground friction forces acting on the snake robot are *anisotropic*, i.e. that the friction coefficient characterizing the ground friction forces in the normal (sideways) direction of each joint is larger than the friction coefficient characterizing the ground friction forces in the tangential (forward) direction of the joint. This property is essential for efficient snake locomotion on a planar surface and is also present in the model of the snake robot presented in Section II. Note that the wheels are able to slip sideways, so they do not introduce nonholonomic constraints in the system.

Each joint module is battery-powered and contains a custom-designed microcontroller card used to control the joint angles. A microcontroller card (the brain card) located in the head of the snake robot transmits joint reference angles to all joint modules over a CAN bus running through the robot. The joint reference angles are calculated on an external computer

Fig. 7. A ring with 12 plastic wheels encloses each joint module in order to give the robot anisotropic ground friction properties.

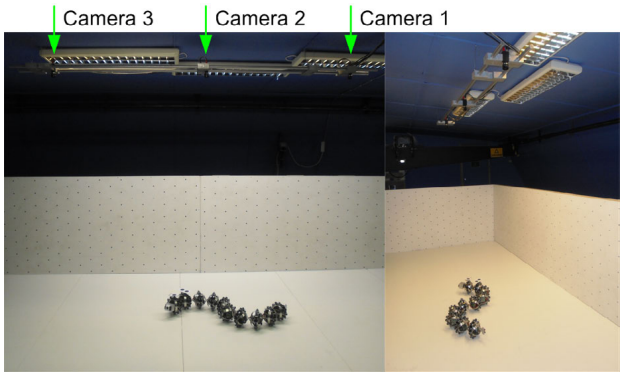

Fig. 8. The experimental setup. Three cameras mounted in the ceiling measured the position of the snake robot on a horizontal surface measuring about 240 cm in width and 600 cm in length.

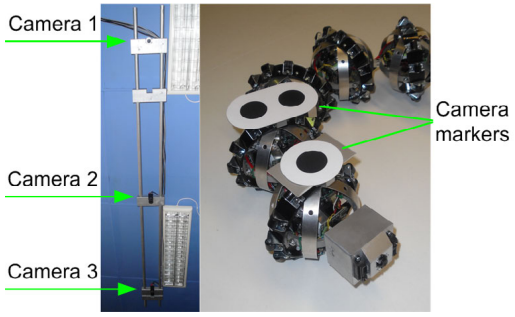

Fig. 9. Left: The firewire cameras mounted in the ceiling above the snake robot. Right: The black markers mounted on the snake robot to allow the position to be tracked by SwisTrack.

in accordance with a defined control strategy and sent to the brain card via a wireless connection based on Bluetooth. The refresh rate for the two reference angles of each joint module is about 20 Hz. The joint torque controller given by (4) and (8) has not been implemented since accurate torque control is not supported by the servo motors installed in the snake robot. Instead, the joint angles are controlled according to a proportional controller implemented in the microcontroller of each joint module.

B. The camera-based position measurement system

During the experiments, the snake robot moved on a white horizontal surface measuring about 240 cm in width and 600 cm in length. This is shown in Fig. 8. In order to measure the 2D position of the snake robot during the experiments, we employed the open source camera tracking software *SwisTrack* [19]. Three firewire cameras (Unibrain Fire-i 520c) were mounted in the ceiling above the snake robot as shown in Fig. 8 and to the left in Fig. 9. The use of multiple cameras allowed for position measurements over a greater distance than the area covered by a single camera. The cameras were mounted facing downwards approximately 218 cm above the floor and 132 cm apart. The distance between the cameras was chosen so that there was a slight overlap between the images from two neighbouring cameras.

SwisTrack was configured to track black circular markers (40 mm in diameter) mounted on the snake robot as shown to the right in Fig. 9. The conversion from the pixel position of a marker to the real-world position (in cm) was conducted by SwisTrack based on a specific calibration method available in this software. SwisTrack estimated the maximum position error to be about 1.9 cm and the average position error to be about 0.6 cm. Each firewire camera was sampled at 15 frames per second. We ran three separate instances of SwisTrack in order to process data from all three cameras and developed our own software in order to merge the output from each SwisTrack instance into the final position measurement of the snake robot. The position of the single marker mounted on the foremost module of the robot was used to represent the measured position of the snake.

C. Layout of the experiment

The aim of the experiment was to investigate the validity of Proposition 1, i.e. to investigate the relationship between the average forward velocity and the controller parameters of the snake robot during lateral undulation. During the experiment, the joint reference angles were calculated on an external computer and sent to the snake robot through the wireless Bluetooth connection. The reference angles corresponding to the horizontal joint motion of the robot were calculated according to (5) with $N = 10$ links. The reference angles corresponding to the vertical joint motion were set to zero. The resulting position of the robot was recorded by the camera system and the average forward velocity was calculated after each run as the travelled distance divided by the travel time.

A typical plot of the measured position of the snake robot from a single run is shown in Fig. 10, which shows that the foremost joint module moves from side to side along the X direction, but has a steady increase in the position along the Y direction. The markers p_{start} and p_{stop} in the plot have been placed near the beginning and near the end of the data set, respectively, at the approximate center point of the cyclic sideways motion of the snake. We used the distance between these two markers to represent the distance travelled by the snake robot and calculated the travel time as the difference in sample time between the position measurements corresponding to the two markers. The average forward velocity of the snake robot was then calculated as

$$\overline{v} = \frac{\sqrt{(p_{\text{stop},x} - p_{\text{start},x})^2 + (p_{\text{stop},y} - p_{\text{start},y})^2}}{t_{\text{stop}} - t_{\text{start}}} \tag{26}$$

When the duration, $t_{\text{stop}} - t_{\text{start}}$, of a single run of the robot is long, we conjecture that the accuracy of this velocity estimate will be sufficient for investigating the validity of Proposition 1. We developed a special software based on *Matlab* in order to easily identify the markers p_{start} and p_{stop} in the position plot from each run of the robot.

VI. Experimental results

This section presents the results from the experimental investigation of the validity of Proposition 1.

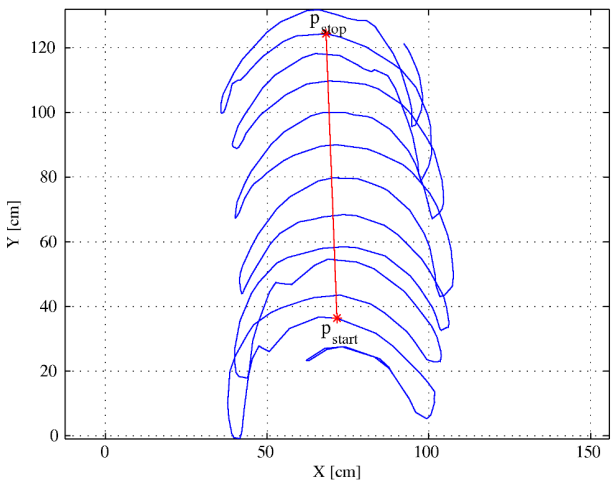

Fig. 10. A typical plot of the measured position of the snake robot during lateral undulation. The distance between the markers p_{start} and p_{stop} represents the distance travelled by the snake robot.

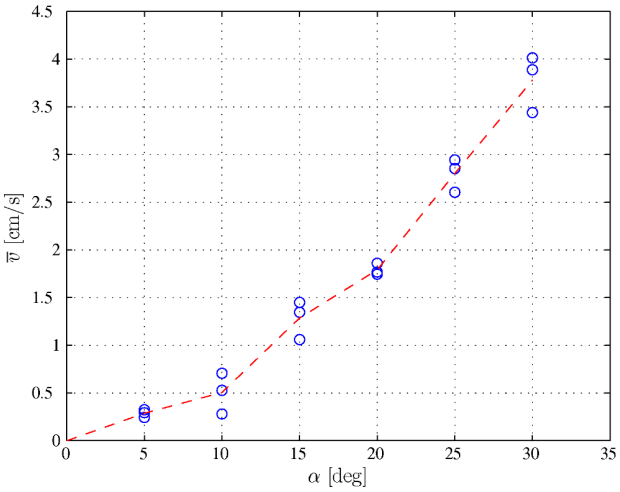

Fig. 12. The average forward velocity of the snake robot from three trials at different values of α. The remaining controller parameters were set to $\omega = 80°$/s, $\delta = 25°$ and $\phi_o = 0°$.

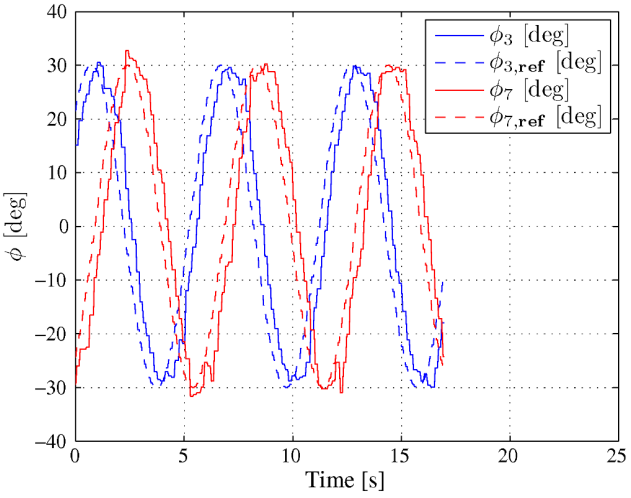

Fig. 11. A plot of the measured (solid) and the corresponding reference angles (dashed) of joint 3 and joint 7 during lateral undulation.

A. Performance of the joint angle controller

In order to show that the joint modules were able to track their joint reference angles, we provide in Fig. 11 a plot of the measured and the corresponding reference angles of two arbitrarily chosen joints (joint 3 and joint 7) during a run of lateral undulation with the snake robot. The plot indicates that the tracking of the joint reference angles is satisfactory.

B. Relationship between the forward velocity and α

Proposition 1 states that the average forward velocity of a planar snake robot is proportional to the squared amplitude of the sinusoidal joint motion, α^2. We investigated the validity of this result by running the snake robot with different values of α and calculating the resulting average forward velocity according to (26). For each value of α, we ran the snake robot three times in order to get multiple velocity measurements. The remaining controller parameters were set to $\omega = 80°$/s, $\delta = 25°$ and $\phi_o = 0°$. Fig. 12 presents the experimental results together with a dashed line between the average of the three velocities measured for each value of α. The plot clearly shows an exponential increase in the forward speed $\overline{v}$ as the amplitude α increases. This is in accordance with Proposition 1.

C. Relationship between the forward velocity and ω

Proposition 1 states that the average forward velocity of a planar snake robot is proportional to the angular frequency, ω, of the joint motion. This result was investigated by running the snake robot with different values of ω and calculating the resulting average forward velocity according to (26). For each value of ω, we ran the snake robot three times in order to get multiple velocity measurements. The remaining controller parameters were set to $\alpha = 30°$, $\delta = 25°$ and $\phi_o = 0°$. Fig. 13 presents the experimental results together with a dashed line between the average of the three velocities measured for each value of ω. The plot clearly shows a linear increase in the forward speed $\overline{v}$ as the frequency ω increases. This is in accordance with Proposition 1.

D. Relationship between the forward velocity and δ

The final result stated in Proposition 1 is that the average forward velocity is maximized by the phase shift δ that maximizes the function k_δ. To investigate the validity of this result, we ran the snake robot with different values of δ to identify the phase shift that produced the highest forward velocity. For each value of δ, we ran the snake robot eight times in order to get multiple velocity measurements. The remaining controller parameters were set to $\alpha = 30°$, $\omega = 80°$/s and $\phi_o = 0°$. Fig. 14 presents the experimental results together with a dashed line between the average of the eight velocities measured for each value of δ. The δ value that maximizes k_δ for $N = 10$ links is $\delta = 24.1°$, and is indicated with a vertical dashed line in Fig. 14. The plot indicates that the phase shift $\delta = 25°$ produced the highest forward velocity.

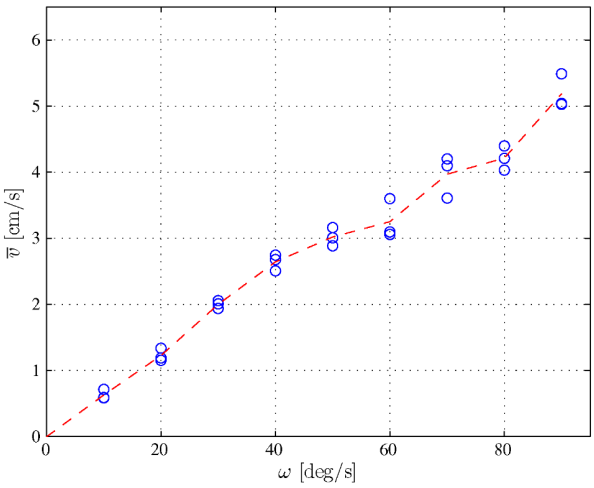

Fig. 13. The average forward velocity of the snake robot from three trials at different values of ω. The remaining controller parameters were set to $\alpha = 30°$, $\delta = 25°$ and $\phi_o = 0°$.

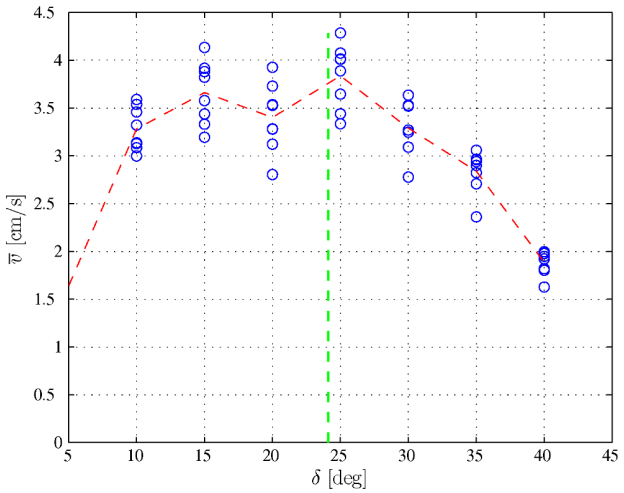

Fig. 14. The average forward velocity of the snake robot from eight trials at different values of δ. The remaining controller parameters were set to $\alpha = 30°$, $\omega = 80°$/s and $\phi_o = 0°$.

This agrees well with the phase shift $\delta = 24.1°$ that maximizes k_δ. The average velocity of the eight trials at $\delta = 25°$ was slightly below 4 cm/s. In summary, the experimental results indicate that Proposition 1 provides a reasonable prediction of the phase shift, δ, that maximizes the average forward velocity of a planar snake robot during lateral undulation.

VII. Conclusions and Future Work

This paper has derived and experimentally investigated a set of fundamental properties of the velocity dynamics of a planar snake robot based on a simplified model of the robot. The properties state that the average forward velocity of a planar snake robot conducting lateral undulation is proportional to 1) the squared amplitude of the sinusoidal joint motion, 2) the angular frequency of the sinusoidal joint motion, and 3) a particular function of the constant phase shift between the joints. Moreover, the phase shift between the joints that maximizes the forward velocity of the snake is given by the phase shift that maximizes the particular phase shift function. The paper has presented an experimental investigation of the validity of these derived properties by measuring the forward velocity of a physical snake robot during lateral undulation. The experimental results supported the theoretical findings. In future work, the authors will employ the derived properties in order to develop and analyse motion planning strategies for snake robots.

References

[1] J. Gray, "The mechanism of locomotion in snakes," *J. Exp. Biol.*, vol. 23, no. 2, pp. 101–120, 1946.

[2] S. Hirose, *Biologically Inspired Robots: Snake-Like Locomotors and Manipulators*. Oxford: Oxford University Press, 1993.

[3] M. Saito, M. Fukaya, and T. Iwasaki, "Serpentine locomotion with robotic snakes," *IEEE Contr. Syst. Mag.*, vol. 22, no. 1, pp. 64–81, February 2002.

[4] G. P. Hicks, "Modeling and control of a snake-like serial-link structure," Ph.D. dissertation, North Carolina State University, 2003.

[5] M. Nilsson, "Serpentine locomotion on surfaces with uniform friction," in *Proc. IEEE/RSJ Int. Conf. Intelligent Robots and Systems*, 2004, pp. 1751–1755.

[6] A. A. Transeth, N. van de Wouw, A. Pavlov, J. P. Hespanha, and K. Y. Pettersen, "Tracking control for snake robot joints," in *Proc. IEEE/RSJ Int. Conf. Intelligent Robots and Systems*, San Diego, CA, USA, Oct-Nov 2007, pp. 3539–3546.

[7] J. Li and J. Shan, "Passivity control of underactuated snake-like robots," in *Proc. 7th World Congress on Intelligent Control and Automation*, June 2008, pp. 485–490.

[8] P. Liljebäck, K. Y. Pettersen, Ø. Stavdahl, and J. T. Gravdahl, "Stability analysis of snake robot locomotion based on poincaré maps," in *Proc. IEEE/RSJ Int. Conf. Intelligent Robots and Systems*, 2009, pp. 3623–3630.

[9] ——, "Controllability analysis of planar snake robots influenced by viscous ground friction," in *Proc. IEEE/RSJ Int. Conf. Intelligent Robots and Systems*, 2009, pp. 3615–3622.

[10] P. A. Vela, K. A. Morgansen, and J. W. Burdick, "Underwater locomotion from oscillatory shape deformations," in *Proc. IEEE Conf. Decision and Control*, vol. 2, Dec. 2002, pp. 2074–2080 vol.2.

[11] K. McIsaac and J. Ostrowski, "Motion planning for anguilliform locomotion," *IEEE Trans. Robot. Autom.*, vol. 19, no. 4, pp. 637–625, August 2003.

[12] K. Morgansen, B. Triplett, and D. Klein, "Geometric methods for modeling and control of free-swimming fin-actuated underwater vehicles," *IEEE Transactions on Robotics*, vol. 23, no. 6, pp. 1184–1199, Dec 2007.

[13] P. Liljebäck, K. Y. Pettersen, Ø. Stavdahl, and J. T. Gravdahl, "A simplified model of planar snake robot locomotion," in *Proc. IEEE/RSJ Int. Conf. Intelligent Robots and Systems*, 2010, accepted.

[14] ——, "Fundamental properties of snake robot locomotion," in *Proc. IEEE/RSJ Int. Conf. Intelligent Robots and Systems*, 2010, accepted.

[15] H. K. Khalil, *Nonlinear Systems*, 3rd ed. Prentice Hall, 2002.

[16] J. A. Sanders, F. Verhulst, and J. Murdock, *Averaging Methods in Nonlinear Dynamical Systems*, 2nd ed., ser. Applied Mathematical Sciences. Springer, 2007, vol. 59.

[17] P. Liljebäck, K. Y. Pettersen, Ø. Stavdahl, and J. T. Gravdahl, "Stability analysis of snake robot locomotion based on averaging theory," in *Proc. IEEE Int. Conf. Decision and Control*, 2010, accepted.

[18] P. Liljebäck, K. Y. Pettersen, and Ø. Stavdahl, "A snake robot with a contact force measurement system for obstacle-aided locomotion," in *Proc. IEEE Int. Conf. Robotics and Automation*, 2010, pp. 683–690.

[19] T. Lochmatter, P. Roduit, C. Cianci, N. Correll, J. Jacot, and A. Martinoli, "Swistrack - a flexible open source tracking software for multi-agent systems," in *IEEE/RSJ Int. Conf. Intelligent Robots and Systems*, 2008, pp. 4004–4010.